14. Raeburn, S. P., Ilton, E. S. & Veblen, D. R. Quantitative determination of the oxidation state of iron in biotite using X-ray photelectron spectroscopy: II. In situ analyses. *Geochim. Cosmochim. Acta* **61,** 4531–4537 (1997).
15. Harris, J., Hutchison, M. T., Hursthouse, M., Light, M. & Harte, B. A new tetragonal silicate mineral occurring as inclusions in lower-mantle diamonds. *Nature* **387,** 486–488 (1997).
16. Mao, H.-K., Shen, G. & Hemley, R. J. Multivariable dependence of Fe-Mg partitioning in the lower mantle. *Science* **278,** 2098–2100 (1997).
17. Wood, B. J. & Rubie, D. C. The effect of alumina on phase transformations at the 660-kilometer discontinuity from Fe-Mg partitioning experiments. *Science* **273,** 1522–1524 (1996).
18. Disko, M. M., Ahn, C. C. & Fultz, B. *Transmission Electron Energy Loss Spectrometry in Materials Science* (Minerals, Metals & Materials Soc., Warrendale, IL, 1992).
19. Garvie, L. A. J. & Craven, A. J. High-resolution parallel electron energy-loss spectroscopy of Mn $L_{2,3}$-edges in inorganic manganese compounds. *Phys. Chem. Minerals* **21,** 191–206 (1994).
20. Garvie, L. A. J. & Buseck, P. R. in *Boron Mineralogy, Petrology and Geochemistry* (eds Grew, E. S. & Anovitz, L. M.) 821–843 (*Reviews in Mineralogy* vol. 33, Mineralogical Soc. Am., Washington DC, 1996).
21. Garvie, L. A. J., Craven, A. J. & Brydson, R. Use of electron-energy loss near-edge fine structure in the study of minerals. *Am. Mineral.* **79,** 411–425 (1994).
22. Egerton, R. F. *Electron Energy-Loss Spectroscopy in the Electron Microscope* 2nd edn (Plenum, New York, 1996).
23. van der Laan, G. & Kirkman, I. W. The 2p absorption spectra of 3d transition metal compounds in tetrahedral and octahedral symmetry. *J. Phys.: Condens. Matter.* **4,** 4189–4204 (1992).
24. Browning, N. D., Chisholm, M. F. & Pennycook, S. J. Atomic-resolution chemical analysis using a scanning transmission electron microscope. *Nature* **366,** 143–146 (1993).
25. Bradley, J. P. Nanometer-scale mineralogy and petrography of fine-grained aggregates in anhydrous interplanetary dust particles. *Geochim. Cosmochim. Acta* **58,** 2123–2134 (1994).
26. Colliex, C. New trends in STEM-based nano-EELS analysis. *J. Electron Microsc.* **45,** 44–50 (1996).
27. Czank, M., Mayer, J. & Klein, U. Electron spectroscopic imaging (ESI): A new method to reveal the existence of nm-scale exsolution lamellae. *Eur. J. Mineral.* **9,** 1199–1206 (1997).
28. Righter, K. & Carmichael, I. S. E. Mega-xenocrysts in alkali olivine basalts: Fragments of disrupted assemblages. *Am. Mineral.* **78,** 1230–1245 (1993).
29. McGuire, A. V., Francis, C. A. & Dyar, M. D. Minerals standards for electron microprobe analysis of oxygen. *Am. Mineral.* **77,** 1087–1091 (1992).
30. Gudmundsson, G. & Holloway, J. R. Activity–composition relationships in the system Fe-Pt at 1300 and 1400 °C and at 1 atm and 20 kbar. *Am. Mineral.* **78,** 178–186 (1993).
31. Van Aken, P. A., Liebscher, B. & Styrsa, V. S. Quantitative determination of iron oxidation states in minerals using Fe $L_{2,3}$-edge electron energy-loss near-edge structure spectroscopy. *Phys. Chem. Miner.* **5,** 323–327 (1998).

Acknowledgements. We thank P. Rez and J. Bradley for discussions, and K. Righter, D. Canil and G. Gudmundsson for providing us with samples. This work was supported by the Earth Sciences Division of the US NSF.

Correspondence and requests for materials should be addressed to L.A.J.G. (e-mail: lgarvie@asu.edu).

Mice lacking melanin-concentrating hormone are hypophagic and lean

Masako Shimada*, Nicholas A. Tritos†, Bradford B. Lowell*, Jeffrey S. Flier* & Eleftheria Maratos-Flier‡

** Division of Endocrinology, Beth Israel Deaconess Medical Center, 330 Brookline Avenue, Boston, Massachusetts 02115, USA*
† Research Division, Joslin Diabetes Center, 1 Joslin Place, Boston, Massachusetts 02215, USA

Feeding is influenced by hypothalamic neuropeptides that promote (orexigenic peptides) or inhibit feeding[1]. Of these, neuropeptide Y (NPY) in the arcuate nucleus[2] and melanin-concentrating hormone (MCH)[3] and orexins/hypocretins[4,5] in the lateral hypothalamus have received attention because their expression is increased during fasting and because they promote feeding when administered centrally. Surprisingly, absence of the orexigenic neuropeptide NPY fails to alter feeding or body weight in normal mice[6]. As deficiency of a single component of the pathway that limits food intake (such as leptin or receptors for melanocortin-4)[7,8] causes obesity, it has been suggested that orexigenic signals are more redundant than those limiting food intake[7,8]. To define further the physiological role of MCH and to test the redundancy of orexigenic signals, we generated mice carrying a targeted deletion of the MCH gene. MCH-deficient mice have reduced body weight and leanness due to hypophagia (reduced feeding) and an inappropriately increased metabolic rate, despite their reduced amounts of both leptin and arcuate nucleus pro-opiomelanocortin messenger RNA. Our results show that MCH is a critical regulator of feeding and energy balance which acts downstream of leptin and the melanocortin system, and that deletion of a gene encoding a single orexigenic peptide can result in leanness.

The MCH gene was disrupted in embryonic stem cells by homologous recombination using a targeting vector in which exons 1–3 of the MCH gene were replaced by a construct consisting of phosphoglycerate kinase (PGK) promoter and the neomycin-resistance (*neo*^{r}) gene (PGK-*neo*^{r}) (Fig. 1a). Two embryonic stem cell lines with correctly targeted recombination were detected by Southern blot analysis, and a line of mice with a disrupted MCH gene (*MCH*$^{-/-}$) was established (Fig. 1b). Reverse transcription with polymerase chain reactions (RT-PCR; Fig. 1c) and *in situ* hybridization (Fig. 1d) confirmed disruption of the MCH gene in *MCH*$^{-/-}$ mice. In addition, immunocytochemistry showed that MCH was not immunostained in the brain of *MCH*$^{-/-}$ mice (data not shown).

MCH$^{-/-}$ mice were born at the expected mendelian frequency, viable into adulthood, and fertile, and they appeared phenotypically

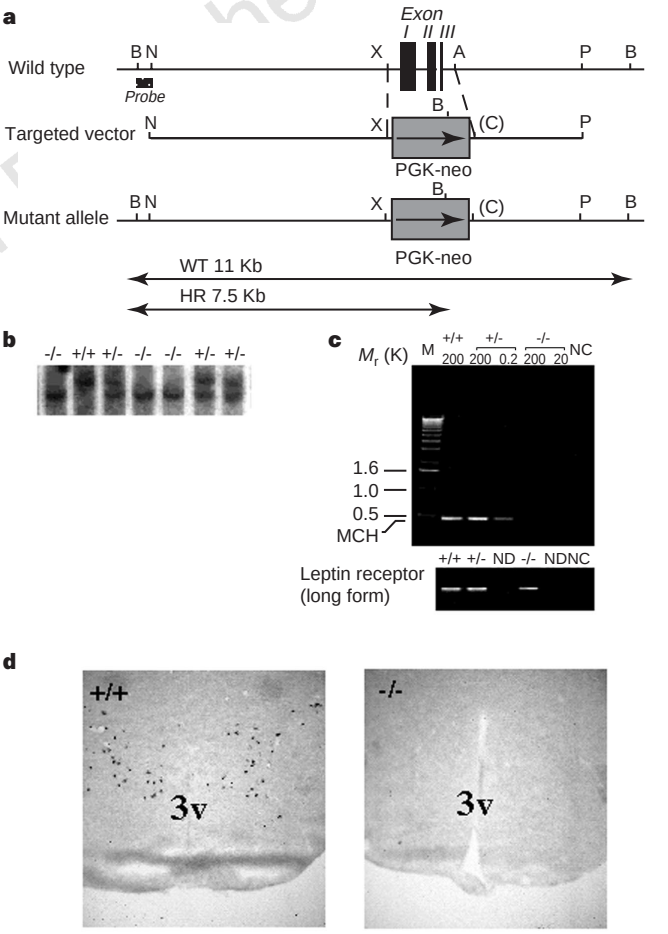

Figure 1 Targeted disruption of the MCH gene in mice. **a**, Top, the targeted region of the MCH gene locus. Middle, the *PGK–neo*^{r} cassette was used to disrupt the MCH gene coding region. Bottom, the expected targeted allele. Restriction enzyme sites: B, *Bgl*II; N, *Nco*I; X, *Xba*I; A, *Afl*; P, *Pst*I; (C), *Cla*I in polylinker. The thick black bar indicates the genomic 320-bp *Bgl*II–*Nco*I probe. WT, wild-type; HR, the homologous recombinant allele. **b**, Southern blot analysis of mouse tail genomic DNA. Genotypes are shown at the top. **c**, Top, detection of MCH mRNA in the hypothalamus using RT-PCR. The mouse genotype and total amount of RNA (in ng) used for RT-PCR in each group is shown at the top. Bottom, RT-PCR analysis, using primers for the long form of the leptin receptor and the same RNA as in the top panel. M, marker; NC, negative control; ND, not done. **d**, *In situ* hybridization with a digoxigenin-labelled riboprobe was used to analyse MCH expression in the hypothalamus of wild-type (left) and *MCH*$^{-/-}$ (right) mice. 3V, third ventricle.

normal by gross inspection except for their reduced size. The mean body weight of both male and female $MCH^{-/-}$ mice was reduced, and this was first apparent between 4 and 5 weeks of age. At 17 weeks of age, male $MCH^{-/-}$ mice weighed 28% less (Fig. 1a) and female $MCH^{-/-}$ mice weighed 24% less (Fig. 2b) than control mice; weights of heterozygous $MCH^{+/-}$ mice tended to be slightly but not significantly lower than weights of control mice (Fig. 2a, b). Carcass analysis showed that $MCH^{-/-}$ mice had a reduced triglyceride content; they were leaner than control littermates (Fig. 2c). We measured nose–anus length of male mice at 16 weeks of age; this measurement did not vary between groups ($MCH^{+/+}$, 9.2 ± 0.1; $MCH^{-/-}$, 9.1 ± 0.1 cm; $n = 6$ in each group).

The reduced body weight and lean phenotype were associated with hypophagia, as 6-week-old $MCH^{-/-}$ mice ingested 12% fewer calories than control mice over a 24-hour period (Fig. 2d). The entire reduction in food intake occurred during the dark cycle, and the amount of food consumed during the light period, although a small fraction of total daily intake, was significantly increased compared with control animals, indicating that MCH may exert its primary effect on feeding during the dark period (Fig. 2d). However, as $MCH^{-/-}$ mice consumed most of their calories during the dark cycle, like normal mice, it seems that MCH is not necessary for the normal diurnal feeding pattern (Fig. 2d). Consistent with their lean phenotype, the $MCH^{-/-}$ mice showed decreased leptin levels, being 51%, 59% and 42% of control levels at 12:00, 18:00 and 24:00, respectively ($P < 0.05$ versus control) (Fig. 3a).

As MCH has been proposed to play a role in motivated behaviours, we studied the behaviour of $MCH^{-/-}$ mice using an open-field locomotion test[9], in which $MCH^{-/-}$ mice were as active as wild-type controls. Control male mice ($n = 6$) crossed 41 ± 6 squares over 5 minutes whereas $MCH^{-/-}$ male mice ($n = 6$) crossed 43 ± 6 squares over the same interval.

We studied potential effects of MCH deficiency on neuroendocrine function. Thyroxine levels ($MCH^{+/+}$ mice, 4.7 ± 0.6 μg dl^{-1}; $MCH^{-/-}$ mice, 5.2 ± 1.2 μg dl^{-1}; mean ± s.e.m.) and corticosterone levels ($MCH^{+/+}$ mice, 16.9 ± 1.5 ng ml^{-1}; $MCH^{-/-}$ mice, 14.7 ± 1.3 ng ml^{-1}) measured at 06:00 were not significantly different in 15-week-old male $MCH^{-/-}$ mice and controls. Levels of blood glucose and insulin measured in 15-week-old males were also not significantly different (glucose: $MCH^{+/+}$ mice, 107.7 ± 5.3 mg dl^{-1}; $MCH^{-/-}$ mice, 102.6 ± 5.9 mg dl^{-1}; insulin; $MCH^{+/+}$ mice, 0.99 ± 0.06 ng ml^{-1}; $MCH^{-/-}$ mice, 0.72 ± 0.07 ng ml^{-1}; $n = 7$ each group).

The reduction in body weight in $MCH^{-/-}$ mice exceeded the degree to which food intake was reduced, indicating that increased metabolic rate might contribute to the lower weight. Rectal temperature, an imperfect indicator of metabolic rate, was unchanged, being 37.9 ± 0.03 °C in control animals ($n = 6$) and 37.6 ± 0.04 °C in $MCH^{-/-}$ animals ($n = 6$). We therefore measured the metabolic rate of these mice in the fed state. $MCH^{-/-}$ mice show rates of oxygen consumption that are slightly but not significantly higher than control rates when expressed on a per mouse basis ($MCH^{+/+}$ mice, 1.08 ± 0.06 ml O_2 per min per mouse; $MCH^{-/-}$ mice, 1.14 ± 0.06 ml O_2 per min per mouse). However, the rate of oxygen consumption is increased by 20% in $MCH^{-/-}$ mice when normalized to body mass ($MCH^{-/-}$ mice, 34.1 ± 0.4 ml O_2 per min per kg body weight; $MCH^{+/+}$ mice, 27.8 ± 0.4 ml O_2 per min per kg body weight). Whether expressed per mouse or per kg body weight, this rate of

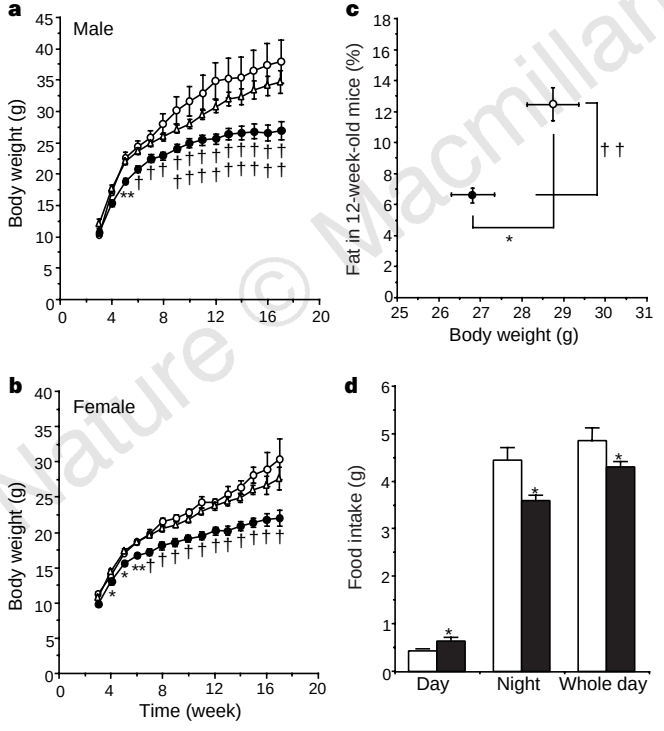

Figure 2 Body weight, fat composition and food intake in $MCH^{-/-}$ and control mice fed on a chow diet. **a**, **b**, Growth curves. Three to four mice were housed per cage. Male: $MCH^{+/+}$, $n = 8$; $MCH^{+/-}$, $n = 19$; $MCH^{-/-}$, $n = 13$. Female: $MCH^{+/+}$, $n = 6$; $MCH^{+/-}$, $n = 28$; $MCH^{-/-}$, $n = 12$. **c**, Percentage of triglycerides relative to body weight in $MCH^{-/-}$ and $MCH^{+/+}$ mice. Open circles, wild-type mice; open triangles, $MCH^{+/-}$ mice; shaded circles, $MCH^{-/-}$ mice. **d**, Food intake by 6-week-old wild-type ($n = 6$; white bars) and $MCH^{-/-}$ ($n = 9$; shaded bars) male mice during the light and dark cycles. Mice were housed individually 4 days before the experiment and the values were determined over a 5-day period. Data are mean intake per day ± s.e.m. Asterisk indicates $P < 0.05$; double asterisk indicates $P < 0.01$; dagger indicates $P < 0.001$; double dagger indicates $P < 0.0001$. Statistical significance was determined by Fischer's PLSD (post-hoc least significant difference).

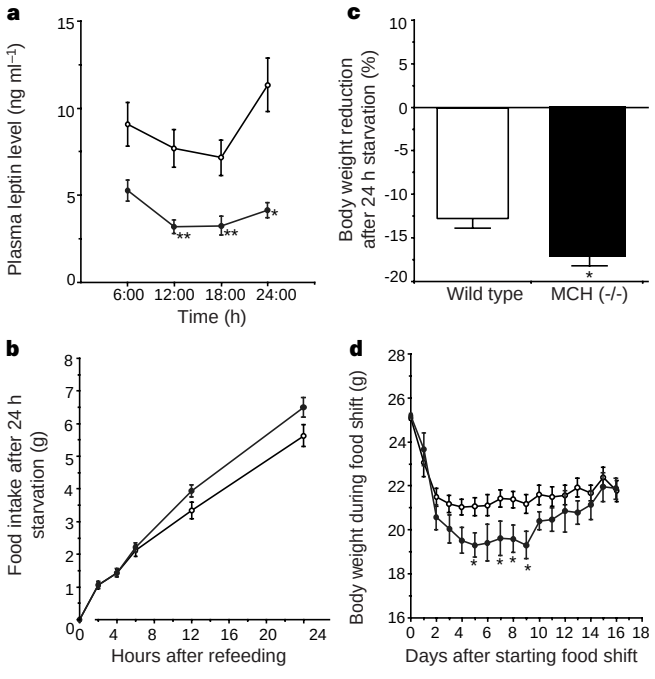

Figure 3 Leptin levels and feeding response in $MCH^{-/-}$ mice. **a**, Leptin levels in 8-week-old male $MCH^{-/-}$ ($n = 6$; filled circles) and $MCH^{+/+}$ ($n = 8$; open circles) mice. Data are means ± s.e.m. **b**, Cumulative food intake in response to starvation in $MCH^{-/-}$ (filled circles) and $MCH^{+/+}$ (open circles) mice. **c**, Body-weight reduction after 24-h starvation. **d**, Response of wild-type (open circles) and $MCH^{-/-}$ (filled circles) mice to food shift. Asterisk indicates $P < 0.05$; double asterisk indicates $P < 0.01$. Statistical significance was determined by Fischer's PLSD.

oxygen consumption may reflect an impaired ability of $MCH^{-/-}$ mice to appropriately regulate their metabolic rate in response to their reduced feeding and lower amounts of leptin (see below). Thus, MCH deficiency promotes weight loss by reducing feeding and may also limit the normal suppression of metabolic rate during food restriction. This combination of results was predicted for $NPY^{-/-}$ mice on the basis of the results of intracerebral injections of this neuropeptide, but mice deficient in NPY showed no such defects[6].

We studied the response of $MCH^{-/-}$ mice to food deprivation. $MCH^{-/-}$ mice responded to 24 hours of starvation with compensatory hyperphagia equal to that of wild-type mice (Fig. 3b). Thus, like NPY[6], MCH is not essential for the hyperphagic response to starvation. However, two lines of evidence indicate that MCH deficiency may create susceptibility to the adverse effects of starvation. First, when age-matched mice were starved for 24 hours, weight loss was greater in $MCH^{-/-}$ mice than in controls ($17.0 \pm 1.0\%$ vs $12.8 \pm 0.9\%$ weight loss, respectively; $n = 6$, $P < 0.05$) (Fig. 3c). Second, when age-matched mice were starved for 48 hours, 3 of 4 $MCH^{-/-}$ but 0 of 4 $MCH^{+/+}$ mice died during the last 4 hours of the fast. The precise basis for these adverse effects of starvation is not yet known, but inappropriate levels of thermogenesis, coupled with reduced initial fat stores, would be expected to cause greater weight loss, and earlier death, in the absence of food intake.

To further explore the response to altered food availability, we used a restricted-feeding paradigm[10]. Food was offered only during the light cycle, between 11:00 and 15:00, to 7-week-old mice. Over a 9-day period, wild-type controls responded to this stress with a 16% reduction in body weight, whereas $MCH^{-/-}$ mice showed 23% weight loss ($P < 0.05$) (Fig. 3d). In contrast, food intake fell to the same degree in wild-type and $MCH^{-/-}$ mice (data not shown), consistent with the possibility that MCH deficiency causes increased thermogenesis under these circumstances.

The hypophagia and leanness of $MCH^{-/-}$ mice led to the production of lower leptin levels, which should cause hyperphagia. However, in the context of MCH deficiency, low leptin levels resulted in decreased rather than increased food intake, indicating that MCH may be essential for the hyperphagic response to leptin deficiency under these conditions. We also examined the effect of exogenous leptin on $MCH^{-/-}$ mice. Leptin was injected at a dose of 1 μg per g body weight twice a day for 2 days. Leptin was able to reduce both food intake and body weight[11] within the initial 24-hour period (Fig. 4). The initial response of $MCH^{-/-}$ mice to leptin was twice that of wild-type mice ($P < 0.05$). This exaggerated response to exogenous leptin, which was also seen in $NPY^{-/-}$ mice, was attenuated by day 2. As leptin inhibits food intake in $MCH^{-/-}$ mice, suppression of MCH is unlikely to be the mechanism by which leptin inhibits food intake in normal mice. Furthermore, MCH may, either directly or indirectly, oppose the effect of leptin in diminishing food intake.

Finally, to assess the state of hypothalamic compensation in response to both MCH deficiency and lower leptin levels, we studied hypothalamic expression of mRNAs encoding four other appetite-regulating neuropeptides in $MCH^{-/-}$ mice, namely NPY, orexin[4], Agouti-related protein (AGRP)[12,13] and pro-opiomelanocortin (POMC)[14,15]. Expression of NPY and AGRP in the arcuate nucleus and of orexin in the lateral hypothalamus remained unchanged in $MCH^{-/-}$ mice in the fed state. However, expression of POMC in the arcuate nucleus was markedly suppressed (decreased by 63% compared with controls; $P < 0.006$) (Fig. 5). As leptin is a positive regulator of arcuate POMC expression[16,17] the reduced POMC expression could result from lower leptin levels, which, in turn, result from a lean body composition. Lower leptin amounts did not increase NPY expression in $MCH^{-/-}$ mice but did in wild-type mice[18]. These results might indicate that POMC expression is more sensitive to the reduction in leptin levels than is NPY expression. Alternatively, MCH deficiency could reduce arcuate POMC expression directly, through the loss of direct innervation of arcuate POMC-expressing neurons by MCH-expressing neurons; MCH immunoreactivity is seen in the arcuate nucleus of wild-type mice[19], consistent with bidirectional communication between POMC- and MCH-expressing systems. There are bidirectional connections between arcuate neurons expressing NPY, AGRP and POMC and lateral hypothalamic neurons expressing MCH and orexins[20]. The lower expression of arcuate POMC, which in other contexts promotes hyperphagia and obesity[21], might be expected to limit the consequences of MCH deficiency. However, our results show that the ability of low arcuate POMC expression (and/or a low POMC:AGRP ratio) to cause hyperphagia and obesity is limited in the absence of an intact MCH gene.

Our $MCH^{-/-}$ mice have a deletion of the entire coding region of the MCH gene, which also encodes the neuropeptides EI and GE[22]. There is little information available on the biological role of these two peptides; direct administration of either peptide alone or in combination in rats has no effect on eating behaviour (E.M.-F., unpublished observations). In theory, the phenotypes of $MCH^{-/-}$ mice could result from deficiency of any or all of these peptides.

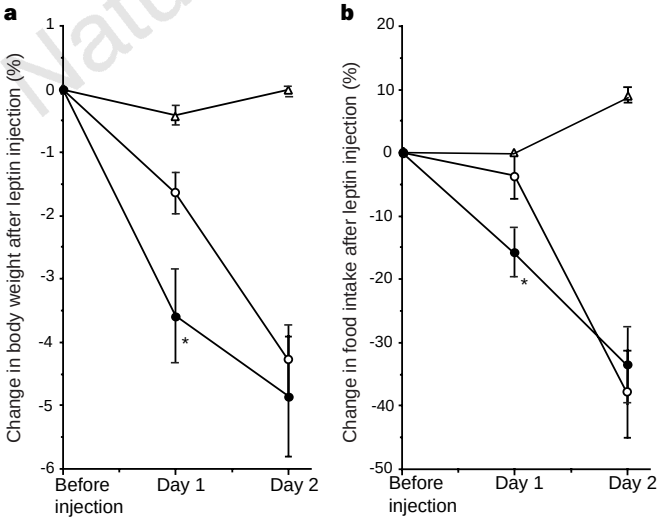

Figure 4 Response of six $MCH^{+/+}$ (open circles) and six $MCH^{-/-}$ mice (shaded circles) to recombinant mouse leptin, administered at a dose of 1 μg per g body weight twice daily (09:00 and 18:00), vs saline control ($n = 3$; triangles). Values for **a**, the change in body weight and **b**, the change in food intake are the per cent change from a 7-day baseline period. Asterisk indicates $P < 0.05$. Statistical significance was determined by Fischer's PLSD.

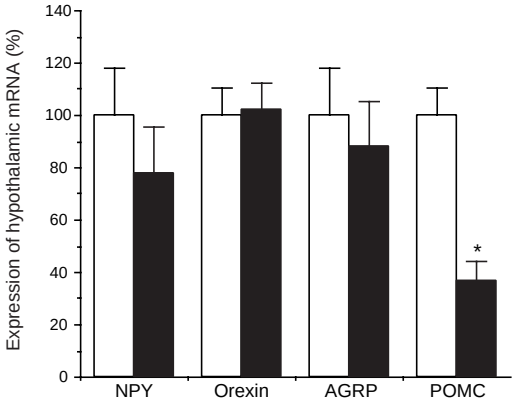

Figure 5 Expression of neuropeptide mRNAs in hypothalami of 24-week-old wild-type ($n = 6$; white bars) and $MCH^{-/-}$ ($n = 6$; shaded bars) mice. Asterisk indicates $P < 0.006$. Statistical significance was determined with the Mann–Whitney test.

However, given the ability of MCH to promote feeding[3,23] and the absence of evidence that NEI and NGE promote such an effect, it is reasonable to assume that MCH deficiency is the primary, or even sole, cause of the phenotype reported here.

MCH is a cyclic 19-amino-acid polypeptide whose expression is limited to the lateral hypothalamus and zona incerta[22,24]. It has been implicated as an important regulator of eating behaviour, because central administration of MCH promotes feeding, and MCH mRNA amounts rise as a result of starvation and leptin deficiency[3]. MCH-expressing neurons are well placed anatomically to participate in feeding behaviour, because they make monosynaptic connections with several areas in the brain involved in integrating inputs related to taste, olfaction and visceral sensations, including the nucleus of the solitary tract, the parabrachial nucleus and the insular and medial prefrontal cortex[24]. MCH-expressing neurons have therefore been suspected to participate in complex integrative behaviours, and the acute feeding response to MCH[3,23] indicated that feeding was among these behaviours. The phenotype of the $MCH^{-/-}$ mouse reported here strongly supports this hypothesis. As the leanness of $MCH^{-/-}$ mice occurs despite reduced expression of leptin and arcuate POMC, which produce obesity when MCH is present[7,21,25], MCH appears to be a critical effector of energy balance downstream of leptin and the POMC/melanocortin system. Further genetic crosses between $MCH^{-/-}$ mice and mice with different causes of obesity will be required to test this hypothesis directly. Finally, as $MCH^{-/-}$ mice are lean, antagonists of MCH action may be effective treatments for obesity.

Methods

Creation of $MCH^{-/-}$ mice. We screened a mouse C129 SvJ P1 genomic library (Genome Systems) using a 250-base-pair (bp) PCR fragment, generated on the basis of the published sequence of the murine MCH gene[26], as a probe. One of three clones was mapped; it consisted of the 16-kilobase (kb) P1 vector and a 72-kb genomic insert containing the MCH coding region between ~25 kb of 5′ and 45 kb of 3′ flanking sequence. We replaced a ~1.8 kb-fragment extending from 340 bp upstream of the translation initiation codon (*Xba*I site) and 200 bp downstream of the stop codon (*Afl*III site)) of this clone with a $PGK\text{–}neo^{r}$ cassette. This targeting vector in pGEM5 (Promega) was linearized at the *Sal*I site and electroporated into the J1 embryonic stem line[27] (cells provided by E. Li and A. Sharp); selection of G418-resistant clones was done as described[27]. We identified targeted clones by Southern blot analysis, using a 320-bp *Bg*II–*Nco*I fragment located 5′ of the targeting vector as a probe; 2 of 68 clones were positive. These positive clones were injected into C57B1/6 embryos at the blastocyst stage. Chimaeric offspring were mated with C57B1/6 mice. Germline transmission of the mutant allele was determined by Southern analysis of mouse tail genomic DNA. One line of mice carrying the disrupted MCH gene was generated, and F_3 hybrids were used in all experiments. We reverse-transcribed 1 μg of total RNA from the hypothalamus of a mouse from each group and amplified aliquots equivalent to 200, 20 and 0.2 ng total RNA by PCR, using the following primers: sense, 5′-ATGGCAAAGATGACTCTCTCT-3′; and antisense, 5′-GACTTGCCAACATGGTCGGTA-3′, as described[26]. *In situ* hybridization was done using a digoxigenin-labelled MHC complementary RNA probe[28].

Studies of $MCH^{-/-}$ mice. Mice were maintained in a daily cycle of 12 h light (06:00–18:00) and 12 h darkness (18:00–06:00) and were allowed free access to chow (Purina Formulab 5008) and water. Total body lipid content was assessed using alcoholic potassium hydroxide digestion with saponification of all fats, neutralization and then enzymatic determination of glycerol (Sigma) as described[29]. Leptin and insulin concentrations were measured by RIA (Linco Research), as were corticosterone and thyroxine levels (ICN). Glucose was measured using a One Touch meter (Lifescan). Rectal temperature was measured with a rectal probe (Yellow Springs Instrument). Oxygen consumption was measured in 20-week-old male wild-type ($n = 4$) and MCH ($n = 4$) mice using an Oxymax 4.93 (Columbus Instruments).

Response to starvation in $MCH^{-/-}$ and $MCH^{+/+}$ mice. We deprived 10-week-old mice ($n = 6$) of food for 24 h, beginning at 09:00; the mice were then allowed free access to chow. To measure cumulative food intake after refeeding, we measured the weight of consumed food at 2, 4, 6, 12 and 24 h after refeeding. Body weights were measured after the 24-h starvation period and after refeeding.

Food-shift experiment. To determine the response of wild-type and $MCH^{-/-}$ mice to food shift, body-weight-matched animals (wild-type male, $n = 7$; $MCH^{-/-}$ male, $n = 4$) were individually housed and allowed free access to chow for only 4 h during the light cycle (11:00–15:00) for 16 days[10]. Body weights were measured at 11:00. Animals were allowed free access to water during the period.

Response to leptin. To determine the response to leptin, mice were injected intraperitoneally with recombinant mouse leptin (Eli Lilly) at a dose of 1 μg per g body weight twice daily (09:00 and 18:00). Three control mice were injected with saline.

Expression of hypothalamic mRNAs. Mice were killed at 09:00 by administration of pentobarbital and were perfused transcardially first with saline and then with 10% buffered formalin. *In situ* hybridization was done with probes for NPY, POMC, AGRP and orexin mRNAs. The images captured on film were quantified with a computing densitometer (Molecular Dynamics) and ImageQuant Software (Molecular Dynamics). We integrated the absorbance in rectangular areas encompassing each nucleus of interest (arcuate nucleus for NPY, POMC and AGRP, and lateral hypothalamus for orexin) over each set of brain sections, and subtracted background density from an adjacent area without specific hybridization signal. We determined statistical significance with the Mann–Whitney test.

Received 15 July; accepted 5 October 1998.

1. Flier, J. S. & Maratos-Flier, E. Obesity and the hypothalamus: novel peptides for new pathways. *Cell* **92,** 437–440 (1998).
2. Dryden, S., Frankish, H., Wang, Q. & Williams, G. Neuropeptide Y and energy balance: one way ahead for the treatment of obesity? *Eur. J. Clin. Invest.* **24,** 293–308 (1994).
3. Qu, D. *et al.* A role for melanin-concentrating hormone in the central regulation of feeding behaviour. *Nature* **380,** 243–247 (1996).
4. Sakurai, T. *et al.* Orexins and orexin receptors: a family of hypothalamic neuropeptides and G protein-coupled receptors that regulate feeding behavior. *Cell* **92,** 573–585 (1998).
5. de Lecea, L. *et al.* The hypocretins: hypothalamus-specific peptides with neuroexcitatory activity. *Proc. Natl Acad. Sci. USA* **95,** 322–327 (1998).
6. Erickson, J., Clegg, K. & Palmiter, R. Sensitivity to leptin and susceptibility to seizures of mice lacking neuropeptide Y. *Nature* **381,** 415–418 (1996).
7. Zhang, Y. *et al.* Positional cloning of the mouse ob gene and its human homologue. *Nature* **372,** 425–432 (1994).
8. Huszar, D. *et al.* Targeted disruption of the melanocortin-4 receptor results in obesity in mice. *Cell* **88,** 131–141 (1997).
9. Krezel, W. *et al.* Impaired locomotion and dopamine signaling in retinoid receptor mutant mice. *Science* **279,** 863–867 (1998).
10. Ahima, R. S., Prabakaran, D. & Flier, J. S. Postnatal leptin surge and regulation of circadian rhythm of leptin by feeding. Implications for energy homeostasis and neuroendocrine function. *J. Clin. Invest.* **101,** 1020–1027 (1998).
11. Halaas, J. *et al.* Weight reducing effect of the plasma protein encoded by the obese gene. *Science* **269,** 543–546 (1995).
12. Ollmann, M. M. *et al.* Antagonism of central melanocortin receptors *in vitro* and *in vivo* by Agouti-related protein. *Science* **278,** 135–138 (1997).
13. Shutter, J. R. *et al.* Hypothalamic expression of ART, a novel gene related to agouti, is up-regulated in obese and diabetic mutant mice. *Genes Dev.* **11,** 593–602 (1997).
14. Tsujii, S. & Bray, G. A. Acetylation alters the feeding response to MSH and beta-endorphin. *Brain Res. Bull.* **23,** 165–169 (1989).
15. Fan, W., Boston, B. A., Kesterson, R. A., Hruby, V. J. & Cone, R. D. Role of melanocortinergic neurons in feeding and the agouti obesity syndrome. *Nature* **385,** 165–168 (1997).
16. Thornton, J. E., Cheung, C. C., Clifton, D. K. & Steiner, R. A. Regulation of hypothalamic proopiomelanocortin mRNA by leptin in ob/ob mice. *Endocrinology* **138,** 5063–5066 (1997).
17. Mizuno, T. M. *et al.* Hypothalamic pro-opiomelanocortin mRNA is reduced by fasting in ob/ob and db/db mice, but is stimulated by leptin. *Diabetes* **47,** 294–297 (1998).
18. Ahima, R. S. *et al.* Role of leptin in the neuroendocrine response to fasting. *Nature* **382,** 250–252 (1996).
19. Bittencourt, J. C. & Elias, C. F. Diencephalic origins of melanin-concentrating hormone immunoreactive projections to medial septum/diagonal band complex and spinal cord using two retrograde fluorescent tracers. *Ann. NY Acad. Sci.* **680,** 462–465 (1993).
20. Elias, C. F. *et al.* Chemically defined projections linking the mediobasal hypothalamus and the lateral hypothalamic area. *J. Comp. Neurol.* (in the press).
21. Krude, H. *et al.* Severe early-onset obesity, adrenal insufficiency and red hair pigmentation caused by POMC mutations in humans. *Nature Genet.* **19,** 155–157 (1998).
22. Nahon, J. L. The melanin-concentrating hormone: from the peptide to the gene. *Crit. Rev. Neurobiol.* **8,** 221–262 (1994).
23. Rossi, M. *et al.* Melanin-concentrating hormone acutely stimulates feeding, but chronic administration has no effect on body weight. *Endocrinology* **138,** 351–355 (1997).
24. Bittencourt, J. C. *et al.* The melanin-concentrating hormone system of the rat brain: an immuno- and hybridization histochemical characterization. *J. Comp. Neurol.* **319,** 218–245 (1992).
25. Montague, C. T. *et al.* Congenital leptin deficiency is associated with severe early-onset obesity in humans. *Nature* **387,** 903–908 (1997).
26. Breton, C., Presse, F., Hervieu, G. & Nahon, J. L. Structure and regulation of the mouse melanin concentrating hormone mRNA and gene. *Mol. Cell. Neurosci.* **4,** 271–284 (1993).
27. Li, E., Sucov, H. M., Lee, K. F., Evans, R. M. & Jaenisch, R. Normal development and growth of mice carrying a targeted disruption of the alpha 1 retinoic acid receptor gene. *Proc. Natl Acad. Sci. USA* **90,** 1590–1594 (1993).
28. Marks, D. L. *et al.* Simultaneous visualization of two cellular mRNA species in individual neurons by use of a new double *in situ* hybridization method. *Mol. Cell. Neurosci.* **3,** 395–405 (1993).

29. Lowell, B. B. *et al*. Development of obesity in transgenic mice after genetic ablation of brown adipose tissue. *Nature* **366,** 740–742 (1993).

Acknowledgements. We thank J. Mastaitis, C. Behn and C. Lee for technical assistance, J. Elmquist for help in analysing and interpreting brain anatomy, and D. S. Ludwig for the P1 clone used in making the construct for the knockout mice. This work was supported in part by grants from NIH to J.S.F. and E.M.-F., from the American Diabetes Association to E.M.-F., and from Eli Lilly to J.S.F. and E.M.-F., and by the Transgenic Core of the Boston Obesity Nutrition Research Center. M.S. was supported by the Banyu Fellowship in Lipid Metabolism and Atherosclerosis which is sponsored by Banyu Pharmaceutical Co Ltd and the Merck Foundation.

Correspondence and requests for materials should be addressed to E.M.-F. (e-mail: emarat@joslab.harvard.edu).

$GABA_B$ receptors function as a heteromeric assembly of the subunits $GABA_B$R1 and $GABA_B$R2

Kenneth A. Jones, Beth Borowsky, Joe A. Tamm, Douglas A. Craig, Margaret M. Durkin, Meng Dai, Wen-Jeng Yao, Mary Johnson, Caryn Gunwaldsen, Ling-Yan Huang, Cheng Tang, Quanrong Shen, John A. Salon, Kelley Morse, Thomas Laz, Kelli E. Smith, Dhanapalan Nagarathnam, Stewart A. Noble, Theresa A. Branchek & Christophe Gerald

Synaptic Pharmaceutical Corporation, 215 College Road, Paramus, New Jersey 07652, USA

The principal inhibitory neurotransmitter GABA (γ-aminobutyric acid) exerts its effects through two ligand-gated channels, $GABA_A$ and $GABA_C$ receptors, and a third receptor, $GABA_B$ (ref. 1), which acts through G proteins to regulate potassium and calcium channels. Cells heterologously expressing the cloned DNA encoding the $GABA_B$R1 protein exhibit high-affinity antagonist-binding sites[2], but they produce little of the functional activity expected from studies of endogenous $GABA_B$ receptors in the brain. Here we describe a new member of the $GABA_B$ polypeptide family, $GABA_B$R2, that shows sequence homology to $GABA_B$R1. Neither $GABA_B$R1 nor $GABA_B$R2, when expressed individually, activates GIRK-type potassium channels; however, the combination of $GABA_B$R1 and $GABA_B$R2 confers robust stimulation of channel activity. Both genes are co-expressed in individual neurons, and both proteins co-localize in transfected cells. Moreover, immunoprecipitation experiments indicate that the two polypeptides associate with each other, probably as heterodimers. Several G-protein-coupled receptors (GPCRs) exist as high-molecular-weight species, consistent with the formation of dimers by these receptors[3–7], but the relevance of these species for the functioning of GPCRs has not been established. We have now shown that co-expression of two GPCR structures, $GABA_B$R1 and $GABA_B$R2, belonging to the same subfamily is essential for signal transduction by $GABA_B$ receptors.

To find other genes related to the $GABA_B$R1 gene, we searched the expressed sequence tags (ESTs) of GenBank using the $GABA_B$R1 sequence. (Throughout the text, '$GABA_B$R1' refers to the $GABA_B$R1b splice variant.) Two entries had scores that suggested significant homology to $GABA_B$R1. We used oligonucleotide probes from these sequences to isolate a full-length clone from a rat hypothalamic complementary DNA library. Sequence analysis of this new clone showed that it has a 2.8-kilobase open reading frame that is predicted to encode a protein of 940 amino acids. A BLAST search of the GenEMBL database indicated that this amino-acid sequence was most closely related to that of $GABA_B$R1, exhibiting 35% and 41% identity overall and within the predicted transmembrane domains, respectively (Fig. 1a). The structural similarity to $GABA_B$R1 indicated that this sequence might encode a new $GABA_B$ polypeptide, which we refer to as $GABA_B$R2. The next most related sequences were other members of the metabotropic glutamate receptor (mGluR) family, with 21–24% overall amino-acid identity. Like $GABA_B$R1 and other members of the mGluR family[8], $GABA_B$R2 contains a large amino-terminal extracellular domain with regions of homology to bacterial amino-acid-binding proteins.

We studied the distribution of $GABA_B$R2 messenger RNA within the central nervous system by *in situ* hybridization. Strong hybridization signals were observed in regions of the rat brain that have high densities of $GABA_B$-receptor-binding sites[9], such as the hippocampus, medial habenula, thalamus and cerebellum (Fig. 1b–e). There was a high degree of similarity in the distribution and intensity of $GABA_B$R1 and $GABA_B$R2 hybridization signals.

Postsynaptic inhibition of neurons by $GABA_B$-receptor activation is caused by the opening of inwardly rectifying K^+ channels (GIRKs)[10–13]. We assessed the ability of either $GABA_B$R1 or $GABA_B$R2 to regulate K^+ currents in cells transfected with GIRK1 and GIRK4 subunits[14–16]. *Xenopus* oocytes injected with either $GABA_B$R1 or $GABA_B$R2 mRNAs failed to generate GABA-evoked GIRK currents (Fig. 2b). The longer splice variant of $GABA_B$R1, $GABA_B$R1a, did not stimulate GIRK activity either, as reported elsewhere[2,17]. In a mammalian host, HEK293 cells, small agonist-evoked currents (10–50 pA) were observed in 5 of 26 cells expressing $GABA_B$R1; similar weak currents were evoked in 1 of 23 cells expressing $GABA_B$R2. In contrast, large currents were produced in 100% of cells expressing the galanin receptor GalR1 (ref. 18) (Fig. 2i).

The overlapping expression patterns of $GABA_B$R1 and $GABA_B$R2 transcripts in the brain indicated that the corresponding proteins might be co-expressed in individual neurons and that both might be required for functional activity. When $GABA_B$R1 and $GABA_B$R2 were co-injected into oocytes together with GIRK subunits, the application of GABA produced robust K^+ currents (Fig. 2a, b). Responses to GABA were abolished in oocytes pretreated with pertussis toxin, showing that receptor stimulation leads to activation of a heterotrimeric G protein of the $G\alpha_o/G\alpha_i$ class. The GABA-induced currents showed the following properties, which suggest that the currents were mediated by GIRK channels: first, a dependency on a raised external K^+ concentration; second, strong inward rectification; third, a reversal potential (−23 mV) near the predicted equilibrium potential for K^+; and fourth, sensitivity to block by 100 μM Ba^{2+} (Fig. 2c).

The pharmacology of agonists at the $GABA_B$R1/$GABA_B$R2 combination was comparable to that reported for native receptors[19,20]. GABA, baclofen and 3-aminopropylmethyl phosphinic acid (3-APMPA) exhibited half-maximally effective concentrations (EC_{50} values) of 1.3 ± 0.1 ($n = 20$), 3.3 ± 0.4 ($n = 8$), and 0.051 ± 0.003 ($n = 6$) μM, respectively (Fig. 2d, g). Concentration–effect curves for GABA were shifted to the right, in an apparently competitive manner, by well-characterized $GABA_B$-selective antagonists (Fig. 2h). Estimates of affinity of the antagonists CGP54626 (33.1 ± 6.3 nM; $n = 4$) and CGP55845 (2.5 ± 0.2 nM; $n = 6$) for $GABA_B$R1/$GABA_B$R2 were similar to values reported in previous electrophysiological studies using brain tissue[19,20], as well as to those obtained by measuring displacement of radioligand from cells expressing $GABA_B$R1 alone[2].

The appearance of robust functional responses after $GABA_B$R1/$GABA_B$R2 co-expression was also observed in HEK293 cells. Upon co-expression of $GABA_B$R1 and $GABA_B$R2 together with GIRKs, GABA evoked currents in 70 of 81 recorded cells (Fig. 2e, i). These currents were blocked by low concentrations of the competitive $GABA_B$-receptor antagonist CGP55845 (ref. 21) and by the GIRK-channel blocker Ba^{2+} (Fig. 2f), indicating that they resulted from the stimulation of $GABA_B$ receptors and the subsequent activation of GIRKs. Large-amplitude currents were also observed when $GABA_B$R2 was paired with the $GABA_B$R1a splice variant (1,046 ± 247 pA; $n = 9$). To